Improving The Concentrated Solar Power Plant Through Connecting The Modular Parabolic Solar Trough

by

Kabir Abiose

Submitted to the
Department of Mechanical Engineering
in Partial Fulfillment of the Requirements for the Degree of

Bachelor of Science in Mechanical Engineering

at the

Massachusetts Institute of Technology

June 2016

Signature of Author: Signature redacted
Department of Mechanical Engineering
May 13, 2016

Certified by: Signature redacted
Alexander Slocum
Pappalardo Professor of Mechanical Engineering
Thesis Supervisor

Accepted by: Signature redacted
Anette Hosoi
Professor of Mechanical Engineering
Undergraduate Officer

Improving The Concentrated Solar Power Plant Through Connecting The Modular Parabolic Solar Trough

by

Kabir Abiose

Submitted to the Department of Mechanical Engineering
on May 13, 2016 in Partial Fulfillment of the
Requirements for the Degree of

Bachelor of Science in Mechanical Engineering

ABSTRACT

Concentrating solar power (CSP) stands as a promising renewable energy technology with the ability to contribute towards global reduction of carbon emissions. A major obstacle to increased adoption of CSP plants has to do with their high initial investment cost; consequently, there is a powerful desire to find improvements that decrease the initial capital investment for a CSP plant. One such improvement involves connecting modularized parabolic trough segments, each with the same dimensions, decreasing the overall amount of actuators required along with greatly simplifying system control architecture.

This thesis is concerned with the extent to which parabolic solar trough modules can be connected together while still being able to operate to desired accuracy under expected load. Accuracy requirements are calculated, along with expected loads resulting in frictional torque on the trough. These expected loads are combined with a model for the effect of connecting multiple trough modules to generate a relationship between number of chained modules and required torsional stiffness. To verify said model, an experimental setup was designed and constructed to simulate loads due to both trough weight and wind loads.

Thesis Supervisor: Alexander Slocum
Tile: Pappalardo Professor Of Mechanical Engineering

Acknowledgements

First, I express gratitude towards my advisors, Profs. Campbell and Slocum – not only for allowing me to engage with an incredibly exciting project, but also for opening my eyes to how vital experimentation is to accurate design, and for remind me, whether implicitly or explicitly, that a good engineer must always be able to account for the unexpected.

Additionally, I owe thanks to the various people that helped with experimental design and fabrication: Dr. Barbara Hughey (for making me second-guess my whole setup in order for me to truly understand it!), Bill Buckley over at the LMP (for showing me how pernicious improper tolerancing can be on the waterjet), and Matt McCambridge over in D-Lab for some last-minute, late-night machining help.

Last, but never least, I owe the biggest thanks to God and my parents, who have supported me well before MIT, and will hopefully continue to do so well after. So many of the wonderful people I have met during my time here have helped me better understand so many different aspects of the world and of myself, and for that I will always be thankful.

Table Of Contents

1. Introduction

1.1 Concentrating Solar Power

Solar thermal energy production is a promising technology for producing energy with a substantially decreased carbon footprint. There is a significant amount of room for growth in solar thermal technologies: the International Energy Agency notes that solar thermal energy is on pace to account for 11% of global electricity generation by 2050.

Concentrating solar power (CSP) generates solar thermal energy by way of parabolic mirrors that focus solar energy on a receiver tube, storing said energy within a heat transfer fluid to be used in some sort of thermodynamic cycle. These plants are appealing due to their built-in thermal storage capacity: if using some heat-storage medium (like a molten salt), the plant has a buffer of sorts to smooth electricity production and allow for production after sunset. **Figure 1-1** depicts a typical CSP plant setup.

Figure 1-1: A concentrated solar power (CSP) plant. This particular plant (Masdar's Shams 1) consists of rows of parabolic troughs, with a receiver tube running through each. The heat stored by the fluid in this receiver tube is then used to generate electricity through some sort of thermodynamic cycle.

While CSP and other solar thermal technologies provide an initial level of appeal, it is crucial for adoption that these technologies are sufficiently cost-effective: the overall

cost to produce energy must be competitive with conventional methods of electricity generation. CSP plants suffer from high initial investment costs resultant from the land and components required to operate a CSP plant. Therefore, to achieve the aim of increased adoption of CSP, it is imperative to find ways to decrease overall investment cost.

1.2 Eni-MIT Parabolic Solar Trough

MIT, in collaboration with Eni S.p.A and Politecnico di Milano, have produced an improved CSP solar collector design with increased plant efficiency through decreased weight, system reliability, and increased modularity. A smaller-scale segment used for testing is shown in Figure [1-2]; Table [1-1] provides the relevant dimensions that characterize the trough.

Figure 1-2: A test segment of the parabolic solar trough module being developed through the Eni-MIT alliance.

Parameter	Value
Length [m]	12
Width [m]	5.775
Focal length [m]	1.72

Table 1-1: Relevant properties of one segment of the Eni-MIT parabolic solar trough module.

The trough modules are actuated via hydraulic piston: for the power and motion requirements of the trough, hydraulic actuators provide the best performance for minimal cost. Even with improved actuator selection, the control architecture required to operate a trough is relatively intensive: for a set of four hydraulic actuators meant to rotate one trough module, each piston requires two separate solenoid valves in addition to added circuitry to allow for simultaneous operation of each piston. Often, these extra components amount to costs as large as or greater than that of the pistons proper. As such, there is a strong motivation to reduce overall cost by reducing the total number of actuators. Connecting multiple trough modules lends itself well to this goal.

To successfully connect several parabolic trough segments, it is crucial that each segment have a sufficiently high torsional stiffness so as to resist the static and dynamic loads being applied. Any angular deflection due to a load alters the trough's orientation with respect to the sun, leading to a decrease in system efficiency. As a result, any attempt to connect multiple trough modules must ensure the total assembly can sufficiently resist the loads being applied with respect to the accuracy requirement for one module.

1.3 Summary Of Work

In light of the above, the steps this thesis will take towards connecting a set of modular solar trough segments are as follows: first, load capacities for an individual solar trough module will be established. Once the loads on an individual module are quantified, then the effect of connecting multiple modules will be modeled. After using an experimental setup to determine the validity of the generated model, a torsional stiffness can be specified, with a subsequent discussion on concepts designed to increase system stiffness.

2. System Requirements

2.1 Accuracy

Accuracy is of paramount importance to a solar collector: if unable to properly track the sun, then the amount of light reflected to the receiver decreases, reducing system efficiency.

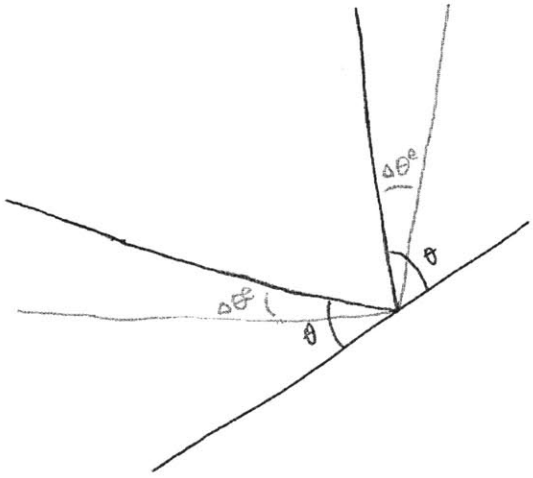

Figure 2-1: The effect of an angular error on overall angular position.

Figure 2-1 details the effect of an angular error in overall light absorbed by the receiver. The sun subtends an angle, θ_s, of approximately 0.52°, providing a spread of 0.52° to the light reflected from the trough. The receiver subtends a larger angle θ_r from the trough, providing a window in which light can be absorbed. For any angular offset θ_e, the spread of light is displaced an additional angle of $2\theta_e$. Moreover, additional errors due to grazing and refraction within the receiver magnify the effect of the error by an additional cosine factor.

To determine a minimum specification for requisite angular accuracy, two approaches may be taken, both providing similar results. In a simple case, we can consider the effect

of an angular displacement for a point on the end of the trough, where θ_r is relatively small (~1.5°). **Figure 2-2** depicts the total room for angular displacement – since there is about 0.5° of space between the perfectly aligned trough and the edge of the spread created by θ_r, we can conclude that, at most, an angular offset of 0.25° would be maintained. However, to account for errors that may accumulate in other parts of the trough (i.e. slope error from how reflective film is applied to the trough), a more conservative error is needed for proper error budgeting. Presuming an angular error of approximately 0.1° and similar errors from in slope and from the receiver, the root-mean-square error is approximately $\sqrt{3} * 0.1° = 0.17°$, leaving overall error less than the maximum tolerable angular offset.

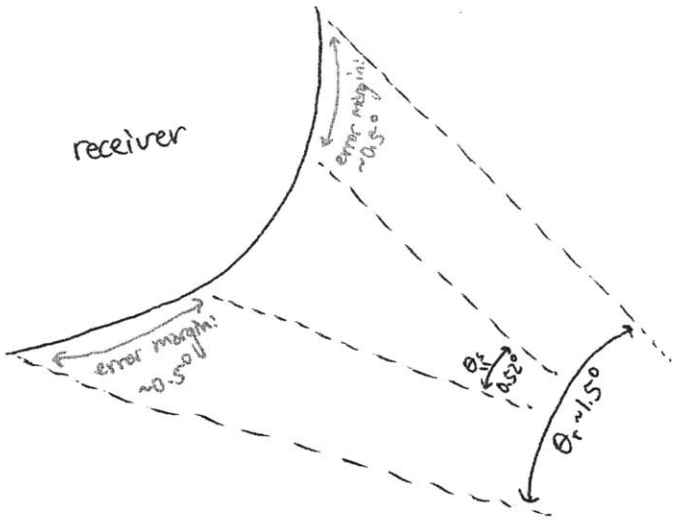

Figure 2-2: Total error margin for angular error.

Alternatively, since efficiency for a particular unit of length changes as a function of location on the parabola, we can write the efficiency as a differential function that is then integrated over the length of the parabola. **Equation [2-1]** describes the efficiency per unit length:

$$\frac{\partial \eta}{\partial x}(\theta_e) = \left[\frac{\theta_r}{2} - \theta_s - 2\theta_e\right] * \cos(\theta_e)$$

The greatest integer function indicates whether or not θ_s is still within the spread defined by θ_r; the cosine takes grazing and refraction errors into account. Using this method, **Figure []** shows how the efficiency varies as a function of angular offset. Using this method, 99% efficiency can be achieved for an angular offset of approximately 0.075°.

2.2 Quantifying Load Capacity

In order to meet angular accuracy specifications, a parabolic trough module must be sufficiently stiff so as to handle the various torques applied. The loads placed on the bearings lead to frictional torques placed on the trough, leading to additional twisting of the parabolic shell. Loads from a combination of module weight and wind combine to create torque that induces torsion on the shell. Quantifying these loads is crucial for developing a torsional stiffness specification for an individual trough module. To achieve this, loads from module weight and wind will be quantified for an individual module, after which the effect of chaining multiple trough modules will be investigated.

2.2.1 Friction Due To Module Weight

As the trough rotates, it is being opposed by frictional torques acting on the bearings supporting the trough. Because the rate of rotation of the trough is discrete (namely, the actuators are acting for only very small amounts of time), we use static friction to determine the expected frictional torque on the module.

The weight of the trough module is supported by two bearings, each of which bearing half of the weight of the trough. The frictional torque can be defined as a function of module weight, bearing geometry, and static coefficient of friction μ via Equation [2-2]:

$$T_{weight} = \frac{\mu \times m_{module} \times g \times r_{bearing}}{2}$$

A singular parabolic trough module weighs approximately 1300 kg, placing a load of 0.5 *12,740 N = 6370 N on each bearing. The sleeve bearings currently in use have an inner diameter of 100 mm, with a bearing radius and coefficient of friction that can vary depending on bearing choice. Table [2-1] compares the frictional torques produced by different types of sleeve bearings based on bearing properties.

Bearing Type	Coefficient Of Friction		Expected Frictional Torque [N*m]	
	Good Operation	Poor Operation	Good Operation	Poor Operation
Cast bronze bearing	0.11	0.21	42	80
Steel-backed, PTFE (Teflon) lined steel bearings	0.05	0.2	16	66
Average ball bearing	0.001	0.0015	0.38	0.57

2.2.2 Wind Loads

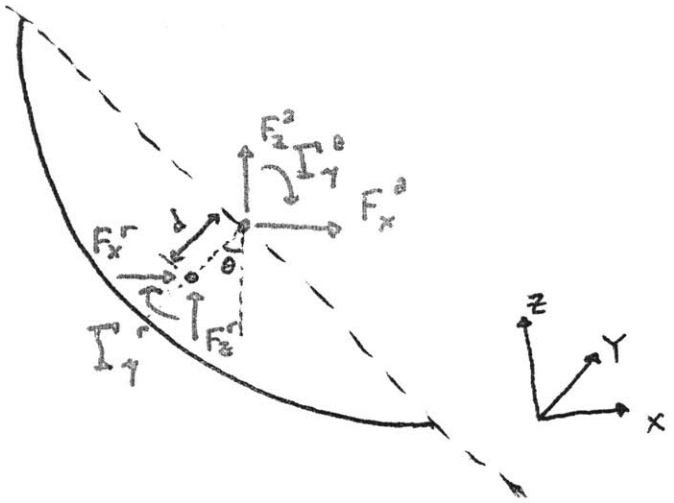

Figure [] depicts the loads placed on the trough due to airflow. Loads caused by airflow (some wind with density ρ and velocity v) act at the aperture of the trough (F_x^a, F_z^a, and T_y^a) at a distance d away from the trough's axle, and are translated to the trough bearings (F_x^r, F_z^r, and T_y^r). Wind loads on the parabolic trough module (with projected area A) act in three different ways:

- Drag force, F_D: relative motion between the trough and airflow leads to a force on the trough due to fluid resistance.
- Lift force, F_L: much like an airfoil, the trough geometry leads to a lift force that acts to either force the trough up or push it down.
- Pitching moment, M_{pitch}: Airflow acting away from the trough's center of rotation creates a moment acting at a distance d away from the trough's axis of rotation.

Since wind loads act at the aperture, the forces at the aperture can be written in terms of wind loads using Equations 2-3 and 2-4:

$$F_x^a = -F_D$$

$$F_z^a = F_L$$

With coefficients of drag, lift, and moment c_D, c_L, and c_M, Equations 2-5 through 2-7 define F_D, F_L, and M_{pitch}:

$$F_D = \frac{1}{2} c_D \rho v^2 A$$

$$F_L = \frac{1}{2} c_L \rho v^2 A$$

$$M_{pitch} = \frac{1}{2} c_M \rho v^2 A$$

The respective coefficients of drag, lift, and moment all depend on the angular orientation of the trough. Moreover, wind loads are affected by the presence of fencing around the solar power plant. Fencing, while providing a measure of security, also creates a "porous jump," leading to a reduction of aerodynamic forces due to a reduction on wind speed.

2.2.2.1 Wind Friction

Drag and lift forces lead to reaction forces at the bearings supporting the trough; this leads to a frictional torque resultant from drag and lift. Equations [2-8 and 2-9] solve the force balance about the trough axle and express F_x^r and F_z^r in terms of aperture reaction forces:

$$F_x^r = -F_x^a$$

$$F_z^r = -F_z^a$$

Equating aperture forces to the wind loads applied and using the fact that the frictional torques from both reaction forces will compound (regardless of the sign of F_D or F_L), **Equation [2-10]** generates bearing frictional torque in terms of F_D, F_L, and $r_{bearing}$:

$$\tau_{wind\ friction} = \mu \left(|F_D| + |F_L|\right) r_{bearing}$$

As F_D and F_L vary over angular position of the collector, the overall frictional torque due to wind will vary as well.

2.2.2.2 Total Moment

In order to find the total moment caused by wind, T_y^r must be determined. Consequently, a moment balance is performed about the trough axle, generating an expression for T_y^r as a function of F_D, F_L, M_{pitch}, d, and θ through **Equation [2-11]**:

$$T_y^r = F_L d \sin\theta + F_D d \cos\theta - M_{pitch}$$

Since the total moment on the trough due to wind is a combination the net moment about the trough axle and total frictional torque at the bearings, we combine Equations [] and [] to leave us with **Equation [2-12]**, an expression for total torque due to wind T_{wind}.

$$T_{wind} = \mu(|F_D| + |F_L|)r_{bearing} + F_L d \sin\theta + F_D d \cos\theta - M_{pitch}$$

From this point, finding total torque on the trough T is simply a matter of summation (**Equation [2-13]**):

$$T = T_{weight} + T_{wind}$$

2.2.2.3 Wind Loads as a Function Of Angle

Since the coefficients determining wind load vary with the angular position θ of the trough, the resultant wind loads on the trough will change with θ as well. Prior work done by researchers at PoliMi used finite-element analysis to generate these coefficients

for the Eni-MIT solar trough. Using this information, **Figure []** shows how c_D, c_L, and c_M change as θ changes, while **Figure []** shows how the loads on the trough vary with θ.

2.2.3 Computing Expected Loads For Normal Operation

In order to compute the expected loads from wind, a wind speed and fixed angular orientation must be set. Wind speed was chosen to be ~12 km/hour, the average expected velocity in the primary working state of the collector. Higher working states allow for drops in efficiency resultant from higher wind speeds, so the state with the least amount of loading is focused on.

To select a reasonable factor for expected force reductions due to a windbreak fence, a relationship between porosity and speed must be specified. For a given porosity f, **Equation [2-14]** provides a wind speed reduction factor based on initial wind speed v_i and final wind speed v_f:

$$\frac{v_f}{v_i} = 1 - f$$

Since wind force is a function of the square of velocity, **Equation [2-15]** produces a force reduction factor:

$$\frac{F_f}{F_i} = (1 - f)^2$$

For ease of calculation, if porosity is set equal to 0.5, then there is a 4x reduction in the force applied. This reduction factor will be applied to calculated wind loads.

To aid in developing a specification for minimum torsional stiffness, the angular position leading to the loads with the largest magnitude must be determined. From

observing Figure [], one concludes that the loads that lead to the largest magnitude of torque on the trough occur *at* $\theta = 0°$.

2.3 The Effect Of Compounding Modules

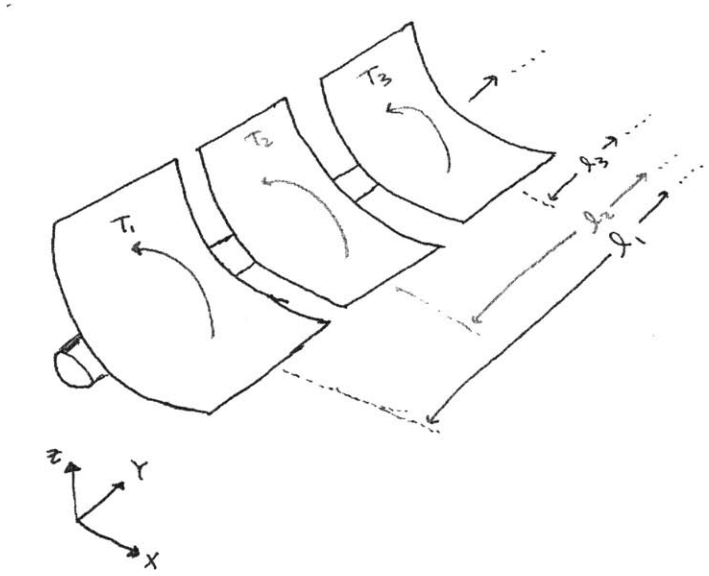

Figure

Figure [] depicts the free-body diagram of multiple chained modules facing torsion due to module weight and wind loads, acting at the bearings supporting each module. Each individual load will place a total twist on the whole assembly, which can be modeled akin to torsion due to a torque applied at the length of some subset of the total set of modules. In other words, for n modules chained together, there will be torsion due to torque applied at the first module (acting over the length of all modules), torsion due to torque applied at the second module (acting over the length of all but the first module), and so on until the last module is reached.

The total maximum twist due to a set of n loads ($T_1 \ldots T_n$) applied at various lengths ($L_1 \ldots L_n$) as a function of shear modulus G and individual module polar moment of inertia I_p is expressed through Equation [2-16]:

$$\theta_{max} = \sum_{i=1}^{n} \frac{T_i L_i}{G I_p}$$

Each individual torque Ti can be treated as the same torque T as determined in Equation [2-13]. L_i denotes the full length Ti is applied over. For any particular module *i*, $L_i = (n - i + 1)l$, where l is individual module length. Performing the summation in Equation [2-16] provides a module multiplication factor for number of modules n described with Equation [2-17]:

$$Module\ multiplication\ factor = 0.5 * n * (n + 1)$$

With this information at hand, we can generate a simple expression for required torsional stiffness for a given number of modules as a function of this module multiplication factor, T, and $\theta_{max} = \theta_e$ in Equation 2-18:

$$\gamma_{req} = (Module\ multiplication\ factor) * \frac{T}{\theta_e}$$

3. Experimentation

To verify the theory presented in the previous section, a setup designed to model trough behavior under load was constructed and tested; subsequent results were used to refine the theory presented and guide design decisions on module stiffening. This section elaborates on the final constructed setup; Appendix A contains additional documentation on the initial experimental setup and preliminary testing preformed.

3.1 Experimental Design

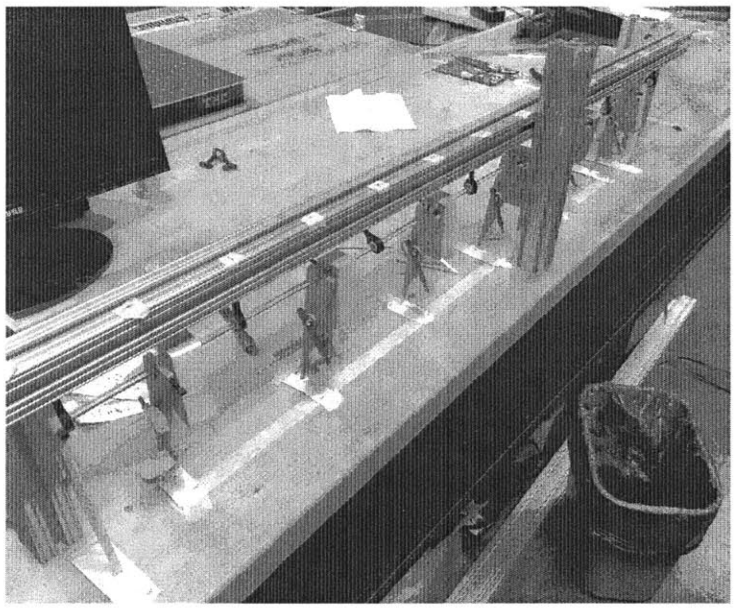

Figure 3-1: Picture of finalized experimental setup.

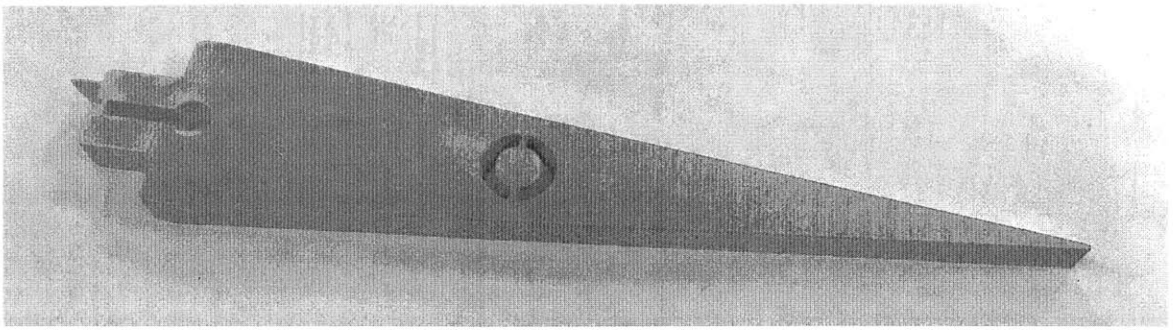

Figure 3-2: One of the Abbe indicators used to measure angular displacement.

Figure 3-1 shows the finalized experimental setup. In place of a trough, a rod was used to measure twist. Polyvinyl chloride (PVC) rod of ¼" diameter over a 42" length was selected to observe noticeable angular deformations and simulate the presence of multiple trough modules. To mimic the simply supported structure of the trough, rod-end bearings were used. To mount this assembly, the rod-end bearings were mounted to an aluminum extrusion frame.

To provide a relatively accurate analog to trough operation at a bench-top scale, expected loads were scaled down by a factor of approximately 10,000 for the experimental setup. Applying a large scaling factor allowed for relatively small weights to be used while allowing for noticeable angular deflection of the rod. Masses with a weight measured to be approximately 135 g were used to simulate frictional torque from module weight.

To measure angular error, indicators shown in **Figure [3-2]** were fabricated to measure Abbe error – for a relatively small change in angle; indicator displacement can be used to find angular displacement via **Equation [3-1]**:

$$\Delta\theta = \sin^{-1}\frac{\Delta x}{l_{indicator}}$$

Moreover, to simulate the effect of changing wind loads at different angles, a lever arm was added to each indicator to apply another set of weights. For a certain frictional torque to be simulated ($\tau_{friction,simulated}$), simulated pitching moment ($M_{pitch,simulated}$), static friction of experimental setup μ_{exp}, rod radius r_{rod}, distance from rod to lever arm axis d_{lever}, and applied weight W, **Equations [3-3 and 3-4]** describe the length and angular position of the lever:

$$\theta_{lever} = \sin^{-1} \frac{\tau_{friction,simulated}}{\sqrt{2}\mu_{exp} r_{rod} W} - \frac{\pi}{4}$$

$$l_{lever} = \frac{M_{pitch,simulated}}{W} - d_{lever} \cos \theta_{lever}$$

To capture loads over multiple angles, the sub-assembly designed to hold weights in placed was adjusted to allow for changes in length and angle. **Figure [3-3]** shows a completed sub-assembly placed on the trough simulator. Masses measured to be approximately 19g were used to simulate wind loading.

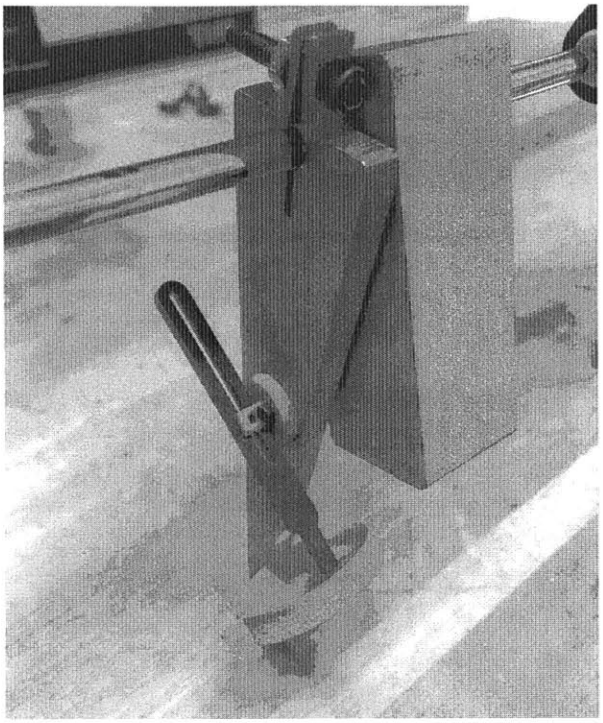

Figure 3-3: A picture of the sub-assembly used to simulate wind loads.

To verify the accuracy of the proposed model, the difference in twist between subsequent modules was observed. Equation [2-16] shows that the difference in twist is not a function of the initial twist applied; thus, the difference in twist is a fixed property of the system that should not vary between trials. As such, this difference is well suited to serve as the comparison between model and experimentation.

3.2 Experimental Procedure

3.2.1 Friction Testing

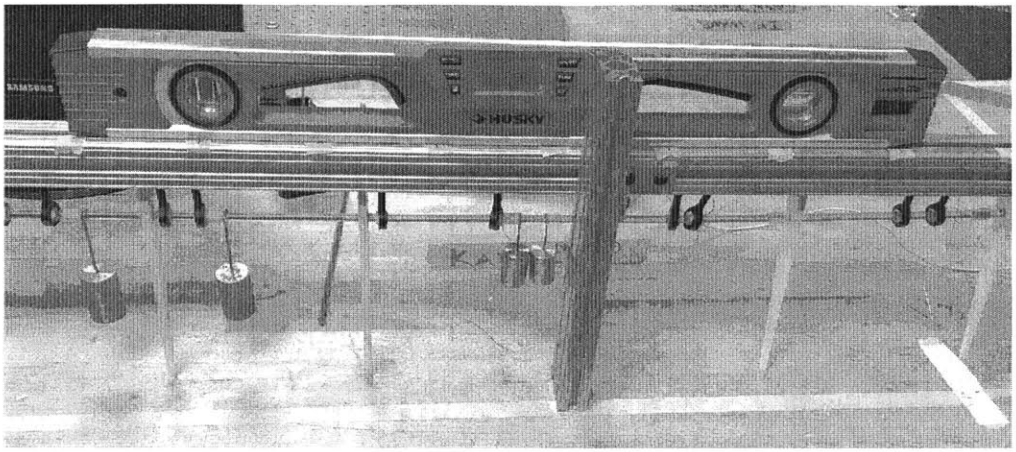

Figure 3-4: Frictional testing was performed by mounting a digital angle gauge on the top of the test setup.

The coefficient of friction for the experimental setup must be determined in order to use the model provided to calculate expected twist. To this end, the experimental setup's coefficient of friction was found by experimentally determining angle of slip θ_{slip} using a digital angle gauge (shown in **Figure [3-4]**). Slight rotations of the experimental frame were noted until the angle at which the setup slipped from the frame was found. After testing, the coefficient of friction was found to be $\mu_{\text{exp}} = 0.279 \pm 0.015$.

3.2.2 Observing Angular Deflection

With weights loading each subsection of the rod, and indicators to note segment rotation (with an additional indicator to note applied torque), the rod was twisted several times: for each segment, the deflection of the indicators at each segment was marked using a strip of paper underneath each indicator. Using this information in conjunction with Equation [3-1] results in the measured angular twist that occurred in the rod.

3.2.3 Changing Angular Orientation

To simulate wind effects, the angle and length of the indicator sub-assembly was varied over a range of several angles. Angular deflection was then observed in the manner described in the previous subsection. Measurements were repeated several times to produce data with reasonable certainty.

3.3 Results

Table [] lists the percent difference between maximum calculated difference in twist and maximum measured experimental twist over several runs. This data is promising for several reasons: first, the overall behavior as a function of segment agrees very strongly with that predicted by the model generated. Not only does the difference in twist grow as segment number increases, but the measured twist in the last two segments of each set of runs is roughly equal – exactly like what the model predicts. Moreover, close observation of Table [] shows a relatively small difference between measured and calculated values; accounting for the uncertainty in experimental measurement makes this difference even smaller. Consequently, we conclude that the experimental setup as constructed serves as a strong validator for the pre-existing model with respect to predicting trough behavior.

However, there is disagreement between experimentation and modeling in the prediction of worst-case loads. **Figure []** plots maximum twist as a function of angular orientation. Comparing this plot to the plot seen in Figure [] leads to a discrepancy of the presence of the worst-case load. While somewhat inconclusive, this should not affect

subsequent work: in applying the experimental scaling factor using Equations [] to find a corresponding load for this deflection, we find that these measurements correspond to an actual load of approximately 50.44 N*m, which is noticeably less than the worst-case condition in Figure [].

4. Torsional Stiffening

Having verified that the model used to generate a specification for torsional stiffness accurately predicts trough behavior; insights from the model will be used to drive design decisions on trough stiffening.

4.1 Current Individual Module Stiffness

Parameter	Value
Weight applied [lbf]	52
Lever arm [in.]	120
Observed rotation [degrees]	0.95
Segment torsional stiffness [N*m/rad]	42,500

To determine the torsional stiffness of the current trough module, a weight was applied to an end of the trough; encoders on the trough were used to measure angular

displacement – as shown in Figure [4-1]. Table [4-1] lists relevant experimental parameters; the resultant torsional stiffness of one module is a third of the test setup (as the module proper is three times as long), or 14,174 N*m/rad. While this is larger than thin-shell approximations for module stiffness might suggest, this is still insufficient for connecting multiple modules: Figure [] shows minimum required torsional stiffness as a function of number of modules; it is clear that additional stiffening will be required.

4.2 Discussion Of Stiffening Schemes

Various methods of stiffening the parabolic solar trough module have been discussed; providing a concrete requirement for torsional stiffness allows the properties of these stiffeners to be quantified. Cost and assembly requirements of each scheme are compared to provide a recommendation.

4.2.1 Torque Tube

Torque tubes are commonplace in parabolic troughs. To provide added stiffness, a rod (commonly made of steel) is mounted to the trough axle so that the trough's rotation is constrained by the rod. To specify the diameter needed such that each module is sufficiently stiff, **Equation [4-1]** can be used:

$$d = 2\sqrt[4]{\frac{2\gamma l}{G\pi}}$$

It is worth noting that for larger chains of modules, the marginal increase in diameter needed to ensure appropriate stiffness is less than the marginal increase at smaller chain sizes.

While a torque tube can provide sufficient torsional stiffness, there is the potential for decreased efficiency. Since the trough axle is in-line with the receiver, placing a torsion tube will lead to shadowing of the receiver, decreasing the amount of light being absorbed around the receiver. Figure [4-2] depicts how these losses accumulate. Using this knowledge, a rough approximation for efficiency with a torque tube in place can be constructed using Equation [4-2]:

4.2.2 Thickened Shell

While attaching a torsionally stiff tube is a viable solution to increasing stiffness, it is also possible to create backing parabolic panels of a larger thickness. The method of calculating the stiffness of a thickened shell is exactly the same as that for the unstiffened shell; using this information, we can generate **Equation [4-3]** to specify shell thickness based on minimum required stiffness:

$$t = \sqrt[3]{\frac{3\gamma l}{GP}}$$

Figure [4-3] plots the desired number of connected trough modules versus the required shell thickness. It is also worth mentioning that thicker shells exacerbate frictional torque issues: a thicker shell drastically increases weight, increasing frictional torque in the bearings and making the issue of torsional stiffness more difficult to solve.

4.2.3 Comparisons

Table [4-2] lists the requisite dimensions for each stiffening scheme as the number of modules is increased.

Cost: more material for thickened shell; abnormal geometry increases cost relative to a rod.

Assembly: shell may be more difficult to assemble, as it has to be constrained over larger area. Various methods of assembly could potentially be used (bolted joints or adhesive) but the torsional tube would require this be over a much smaller area than that of the thickened shell, leading to savings in both material cost and assembly time. Conclusion: prefer the torsion tube for ease of implementation.

5. Conclusion

In summary, the content of this thesis aims to quantify the maximum benefit a CSP plant can gain from decreasing overall capital costs by connecting parabolic trough modules. To do this, a requisite accuracy specification is generated with respect to module efficiency. In conjunction, the expected loads on a singular trough module due to module weight and wind loads are analyzed whilst generating a model to predict total angular error for a given torsional stiffness.

To verify the accuracy of the constructed model, an experimental setup was designed and built to measure angular deflection due to torsional loads. Assemblies simulating module weight and wind loaded were attached to the setup, and angular displacement was measured over a range of different angular orientations. Once finding fair agreement between the model and experimental results, different attempts at stiffening the trough module were observed. For reasons concerning size, cost, effect on performance, and ease of assembly, it is found that a torque tube should allow for stiffness

Appendix A: Initial Experimental Setup

The purpose of the initial experimental setup was to provide initial predictions for trough behavior. The structural components that made up the initial assembly do not differ from the final assembly; **Figure A-1** shows the initial experimental setup.

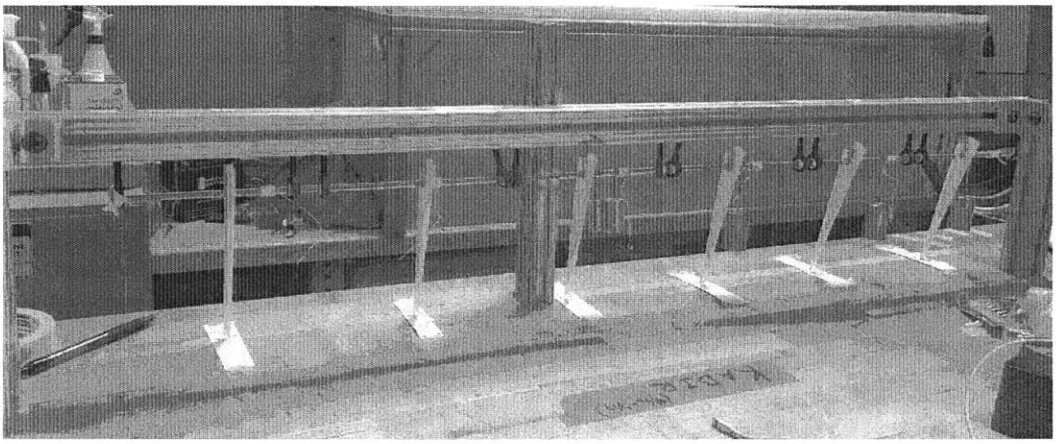

Within Figure A-1 are the initial Abbe indicators prototyped to measure the rod's angular displacement. To minimize possible slip of the indicator (which would have the potential to add substantial error to measurement), the indicators were joined to the rod using a strong adhesive once mounted and properly aligned. Through running initial experiments, it was found that the indicators would often bias data by introducing friction between the indicator tip and the ground. Moreover, errors in adhesive application/general lack of adhesive strength led to an indeterminate amount of slip at the indicators. Due to these errors (and the additional implementation of a lever arm to directly simulate wind loads), the indicators were revised to what is seen in Figure [].

Initial trials also involved twist of a rod while marking deflection of indicators; the most noticeable difference lay in using a partially loaded trough to simulate effects over a smaller section of trough. While the general trend of each trial was found to be the same (and consistent with modeled behavior), a variable scaling factor appeared for each

trial with partially loaded segments, leading to the conclusion that the entire rod must be loaded for accurate predictions. This required additional fabrication, leading to the finalized experimental setup.